Chaos

A new class of out-gap discrete solitons in binary waveguide arrays

Cite as: Chaos **32**, 073113 (2022); https://doi.org/10.1063/5.0079809
Submitted: 24 November 2021 • Accepted: 16 June 2022 • Published Online: 08 July 2022

Minh C. Tran and Truong X. Tran

A new class of out-gap discrete solitons in binary waveguide arrays

Cite as: Chaos **32**, 073113 (2022); doi: 10.1063/5.0079809
Submitted: 24 November 2021 · Accepted: 16 June 2022 ·
Published Online: 8 July 2022

Minh C. Tran[1,2,a)] and Truong X. Tran[3,b)]

AFFILIATIONS

[1]Atomic Molecular and Optical Physics Research Group, Science and Technology Advanced Institute, Van Lang University, 69/68 Dang Thuy Tram Street, 70000 Ho Chi Minh City, Vietnam
[2]Faculty of Applied Technology, School of Engineering and Technology, Van Lang University, 69/68 Dang Thuy Tram Street, 70000 Ho Chi Minh City, Vietnam
[3]Department of Physics, Le Quy Don Technical University, 236 Hoang Quoc Viet Str., 10000 Ha Noi, Vietnam

[a)]trancongminh@vlu.edu.vn
[b)]**Author to whom correspondence should be addressed:** tranxtr@gmail.com

ABSTRACT

We analytically and numerically investigate beyond-band discrete solitons, which present a completely new class of stable localized out-gap solitons with detunings being located beyond the two bands of the linear plane waves in a periodic binary waveguide array. Each of the even and odd components of these discrete solitons does not change its sign across the transverse direction of the binary waveguide array. The even and odd components of these newly found discrete solitons can be approximately presented by two hyperbolic *secant* functions with the only difference in their peaks. This approximation is especially good in the low-intensity regime in which the detuning of these solitons can asymptotically reach the two limits of a linear spectrum. These distinguishing features altogether make the newly found discrete solitons different from all other classes of discrete solitons investigated earlier in binary waveguide arrays. Two transformation rules for constructing even and odd components of these discrete solitons are also found for various combinations of signs of the propagation mismatch σ and nonlinear coefficient γ.

Discrete solitons have been intensively investigated in periodic binary waveguide arrays (BWAs) from both the classical and quantum points of view. Some of the discrete solitons in BWAs are gap ones, while the others are out-gap. The general feature of all these localized structures found earlier in BWAs is that each of their even and odd components constantly changes its sign across the transverse direction of the BWAs. In this work, we investigate beyond-band discrete solitons, which present a completely new class of stable localized out-gap solitons residing beyond the two bands of linear plane waves in BWAs with a distinguishing feature: each of their even and odd components does not change its sign at all across the transverse direction of BWAs. These beyond-band discrete solitons can be well approximated by two hyperbolic functions, especially in the quasilinear regime.

I. INTRODUCTION

Waveguide arrays (WAs) are an interesting periodic system to explore some basic photonic effects, such as discrete diffraction,[1,2] discrete solitons,[1,3] diffractive resonant radiation,[4] just to mention a few. From a practical viewpoint, one can use WAs for creating elements of photonic circuits, such as all-optical routers and logic functions, such as AND and NOT.[5] Moreover, WAs have been widely exploited for simulating well-known effects in nonrelativistic quantum mechanics, for instance, photonic Bloch oscillations[1,6,7] and Zener tunneling,[8] which are all governed by the Schrödinger equation. Surprisingly, binary waveguide arrays (BWAs)—a special class of WAs consisting of two alternating types of waveguides—can be effectively used for mimicking relativistic quantum mechanics effects rooted in the Dirac equations. Indeed, some fundamental relativistic quantum mechanics phenomena, such as *zitterbewegung*,[9] Klein tunneling,[10–12] Dirac solitons,[13–18] topological Jackiw–Rebbi states,[19,20] and electron–positron pair production,[21–23] have been successfully replicated in BWAs.

The discrete gap solitons existing in BWAs have been studied numerically[24–26] and experimentally[27] in the *classical* context. Gap, out-gap solitons, and so-called breathers in BWAs have been found in Refs. 28–30. These discrete gap solitons were first explored in

Ref. 31 for a discrete model of diatomic lattices and later derived in the continuum-limit form for BWAs in Ref. 28, i.e., in the *continuous* system with modulated parameters. In this continuous model studied in Ref. 28, the gap solitons are localized like a bright soliton with a bell-shaped profile, whereas the out-gap solitons are delocalized like a dark soliton with a dip at the center and non-zero background. The so-called discrete on-top breathers reported in Ref. 29 are also out-gap and localized, but they cannot go down in frequency to the linear spectrum. In 2014, the discrete gap solitons in BWAs were explicitly shown for the first time to be optical analogs of one-dimensional Dirac solitons in Ref. 13 in a relativistic quantum Dirac equation with Kerr nonlinearity. Other soliton solutions with a different kind of nonlinearity have also been obtained earlier for the nonlinear Dirac equation.[32] After the derivation of the analytical Dirac soliton solution in BWAs in Ref. 13, its properties and dynamics have been systematically investigated. For instance, the Dirac soliton stability and different scenarios of interaction between two and more Dirac solitons in BWAs have been analyzed in Ref. 14. The generation and dynamics of two-dimensional Dirac solitons in a square binary waveguide lattice have also been studied in Ref. 15. The breathing effect of the higher-order Dirac solitons in BWAs has been demonstrated in Ref. 16. The generation and dynamics of so-called Dirac light bullets in BWAs with both Raman and Kerr nonlinearities have been studied in Ref. 17 where an optical pulse is launched into the system to generate spatiotemporal localized structures. The dynamics of a Dirac soliton and its switching by an extremely weak signal in BWAs with varying propagation mismatches (along the longitudinal axis) between adjacent waveguides have been investigated in Ref. 18. Note also that the inverse Klein tunneling effect has been mimicked in Ref. 12 by launching a Dirac soliton into BWAs.

It is worth mentioning that discrete solitons can also be found in other discrete systems, such as two-component discrete nonlinear Schrödinger lattices, which can be implemented in arrays of bimodal optical waveguides.[33,34] Another class of discrete solitons are so-called discrete embedded solitons, which are localized states embedded in the continuous phonon spectrum and can be found in a model, which describes a one-dimensional array of optical waveguides with both $\chi^{(2)}$ (second-harmonic generation) and $\chi^{(3)}$ (Kerr) nonlinearities.[35]

In this work, we show the existence of *beyond-band discrete* solitons, which present a completely new class of out-gap discrete and stable solitons in BWAs whose properties are totally different from all other discrete solitons found earlier in BWAs. First, these new discrete localized solitons are out-gap with detunings being beyond the two bands of the linear plane waves in BWAs. Second, their even and odd components do not change their respective signs across the BWA in the transverse direction. The remainder of this work is organized as follows: in Sec. II, we briefly re-introduce the governing coupled-mode equations for light beams in BWAs and the Dirac solitons solutions, which have been analytically found in Ref. 13. Then, in Sec. III, we focus on the new class of discrete solitons in the quasilinear regime when the light beam intensity is low enough. In Sec. IV, we study these new discrete solitons in the nonlinear regime of Kerr type when the light beam intensity is enhanced enough. Finally, in Sec. V, we summarize our findings with concluding remarks.

II. GOVERNING EQUATIONS AND GAP DIRAC SOLITON SOLUTIONS

In this section, we would like to briefly re-introduce the Dirac soliton solutions found earlier in Ref. 13. This is relevant because one can later compare the properties of gap Dirac solitons with beyond-band discrete solitons found in this work.

Light evolution in a discrete, periodic BWA consisting of Kerr nonlinear waveguides can be described in the continuous-wave regime by the following well-known dimensionless coupled-mode equations:[10,24]

$$i\frac{da_n(z)}{dz} = -\kappa(a_{n+1} + a_{n-1}) + (-1)^n\sigma a_n - \gamma|a_n|^2 a_n, \qquad (1)$$

where a_n denotes the electric field amplitude in the nth waveguide, z is the longitudinal coordinate, 2σ and κ are, respectively, the propagation mismatch and the coupling coefficient (which is always positive) between two neighboring waveguides of the BWA, and γ is the nonlinear coefficient of waveguides, which is positive for self-focusing, but negative for self-defocusing media. For the sake of simplicity, we suppose that all waveguides in the BWA have the same value for γ. In this work, we study the BWA, which is perfect without any defect as schematically illustrated in Fig. 1(a). In this case, parameter σ is a constant when n discretely runs from $[-(N-1)/2, \ldots, -1, 0, 1, \ldots (N-1)/2]$, where N is the total odd number of waveguides in the BWA. Note that we can always normalize variables of Eq. (1) such that $|\gamma|$ and κ are both equal to unity. Note also that we can use the same BWA to study two cases when σ changes its sign from $1 \leftrightarrow -1$ just by shifting the waveguide position n in Eq. (1) by one. We will get back to this simple but important remark later. System (1) has the Hamiltonian in the following form:[29]

$$H = \sum_n \left(\kappa|a_{n+1} - a_n|^2 + [1 + (-1)^n\sigma]|a_n|^2 + \frac{\gamma}{2}|a_n|^4\right). \qquad (2)$$

The final solution for Dirac solitons in the case when γ and σ are both positive has been obtained in Ref. 13 as follows:

$$\begin{bmatrix} a_{2n}(z) \\ a_{2n-1}(z) \end{bmatrix} = \begin{bmatrix} i^{2n}\frac{2\kappa}{n_0\sqrt{\sigma\gamma}}\,\mathrm{sech}\left(\frac{2n}{n_0}\right)e^{ifz} \\ i^{2n}\frac{2\kappa^2}{n_0^2\sigma\sqrt{\sigma\gamma}}\,\mathrm{sech}\left(\frac{2n-1}{n_0}\right)\tanh\left(\frac{2n-1}{n_0}\right)e^{ifz} \end{bmatrix}, \qquad (3)$$

where parameter n_0 characterizes the Dirac soliton width and the detuning $f = -\sigma + [2\kappa^2/(n_0^2\sigma)]$.

If γ and σ have other combinations of signs, then using the transformation rules explained in detail in Ref. 13 for Dirac solitons in BWAs, we can easily construct the Dirac soliton solutions for these cases.

Note that the analytical Dirac soliton solutions in the form of Eq. (3) are derived under two conditions: (i) the beam must be wide enough such that one can operate in the quasicontinuous limit instead of the discrete one and (ii) $n_0|\sigma| \gg 2\kappa$. Surprisingly, the former condition can be easily satisfied if the width parameter $n_0 \geq 4$, whereas the latter condition is easily satisfied if (i) is held true and if σ is comparable to κ,[9] which is also often met in practice.[11] This second condition also means that $2\kappa^2/(n_0^2|\sigma|) \ll |\sigma|/2$. Therefore, we get the following important relation for the detuning f of the Dirac

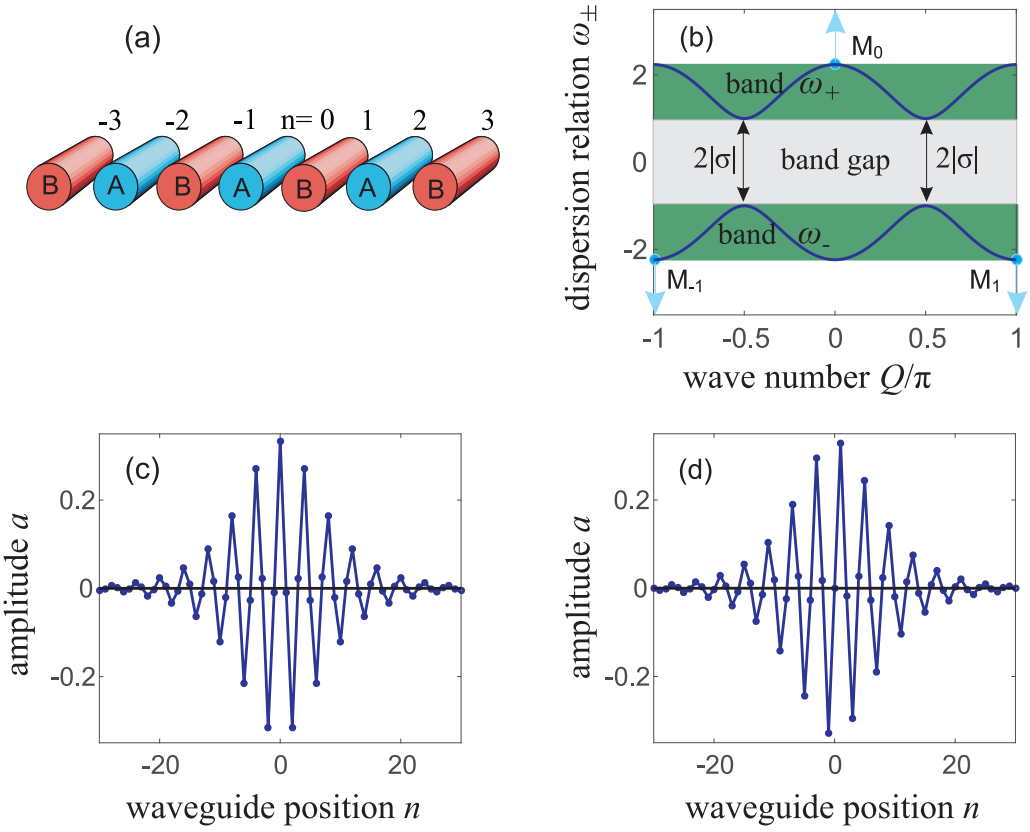

FIG. 1. (a) Illustrative sketch of a BWA. (b) Dispersion curves $\omega_{\pm}$ as two functions of the normalized wave number Q. These two curves create two green bands. Three points M_0, M_{-1}, and M_1 show the limits of the linear detunings $\delta_l = \pm\sqrt{\sigma^2 + 4\kappa^2}$ of beyond-band discrete solitons at $Q = 0$ and $\pm\pi$. In the nonlinear regime, the detunings of beyond-band discrete solitons get the values as schematically shown by three arrows starting from these three points: if $\gamma > 0$, then the upward arrow is taken, whereas if $\gamma < 0$, the two downward arrows are taken. The gray region is the bandgap of plane waves in BWAs. (c) The Dirac soliton profile a_n at $z = 0$ when $\sigma = 1$ and $\gamma = 1$. (d) The Dirac soliton profile at $z = 0$ when $\sigma = -1$ and $\gamma = 1$. Other parameters are $\kappa = 1$ and $n_0 = 6$.

solitons:[17]

$$|\sigma| > f > -|\sigma|. \tag{4}$$

As pointed out in Refs. 9, 13, and 36, by introducing $\Psi_1(n) = (-1)^n a_{2n}$, $\Psi_2(n) = i(-1)^n a_{2n-1}$, and bringing in the continuous transverse coordinate ξ instead of n, Eq. (1) can be converted to the nonlinear Dirac equation in relativistic quantum mechanics for the two-component spinor $\Psi(\xi, z) = (\Psi_1, \Psi_2)^T$ as follows:

$$i\partial_z \Psi = -i\kappa\hat{\sigma}_x\partial_\xi \Psi + \sigma\hat{\sigma}_z\Psi - \gamma G, \tag{5}$$

where the Kerr nonlinearity is considered via the term $G \equiv (|\Psi_1|^2\Psi_1, |\Psi_2|^2\Psi_2)^T$; $\hat{\sigma}_x$ and $\hat{\sigma}_z$ are the well-known Pauli matrices; and T denotes the matrix transposition operator. In the Dirac equation (5), parameter σ is also often referred to as the Dirac mass.[19] By following above-mentioned transformation rules, one can easily convert the discrete soliton solutions (3) of Eq. (1) into the Dirac soliton solution of the Dirac equation (5) as demonstrated in Ref. 19.

Now, it is also important to remind that the Dirac solitons in the form of Eq. (3) are gap solitons. Indeed, by inserting the following *Anstaz* for a plane wave,

$$a_n(Q) \sim \exp[i(Qn - \omega z)], \tag{6}$$

into Eq. (1), one can obtain the dispersion relations in the *linear* regime as follows:[24]

$$\omega_{\pm}(Q) = \pm\sqrt{\sigma^2 + 4\kappa^2\cos^2 Q}, \tag{7}$$

where Q is the normalized wave number of the plane wave, which represents the phase difference between two adjacent waveguides occurred, for instance, due to the inclination of beams inside BWAs. In Fig. 1(b), we plot two dispersion curves $\omega_{\pm}$ described by Eq. (7) in the first Brillouin zone with $-\pi \le Q \le \pi$, which create two green bands therein. As seen from Eq. (7), these two bands ω_- and ω_+ are separated by a gap from $-|\sigma|$ to $|\sigma|$, which is the gray region in Fig. 1(b). At the same time, as pointed out above, the propagation constant parameter f of the Dirac solitons satisfies the relation (4). Therefore, it is now clear that Dirac solitons in the form of Eq. (3) are *gap* solitons[13,17] and are found in the gray region in Fig. 1(b).

As an example, in Fig. 1(c), we show the profile of a Dirac soliton when $\sigma = 1$, $\gamma = 1$ [i.e., the right condition for using a Dirac soliton solution in the form of Eq. (3)], $\kappa = 1$, and $n_0 = 6$. Meanwhile, in Fig. 1(d), we show the profile of a Dirac soliton when $\sigma = -1$ and $\gamma = 1$ using a transformation rule given in Ref. 13. Due to the factor i^{2n} in Dirac soliton solutions in the form of Eq. (3) for both the even components a_{2n} and odd components a_{2n-1}, it is obvious that adjacent *even* components have opposite signs, i.e., $a_{2n}a_{2n+2} < 0$ for all n after dropping the common factor e^{ifz}. This is also true for adjacent odd components where $a_{2n-1}a_{2n+1} < 0$ for all n, apart from the central point at $n = 0$ because the hyperbolic function tanh changes its sign while crossing this point. In other words, both the even and odd components of the Dirac solitons constantly change their signs across the transverse direction of the BWA. Thanks to that, Ψ_1 and Ψ_2 are quite smooth functions with respect to variable ξ (or n), and the derivative $\partial_\xi \Psi$ in the Dirac equation (5) mathematically makes sense. That is the reason why one can construct the soliton solution of the Dirac equation (5) from the discrete soliton solution (3) of Eq. (1), and why the soliton solution in the form of Eq. (3) is called the Dirac soliton in Ref. 13. This is one of the significant differences between Dirac solitons and the new class of beyond-band discrete solitons in BWAs discussed below.

III. BEYOND-BAND DISCRETE SOLITONS IN THE QUASILINEAR REGIME

Now, we use the following *Anstaz* to look for a new class of beyond-band discrete solitons in BWAs:[20]

$$a_n = b_n e^{i\delta z}, \tag{8}$$

where b_n is real and just depends on n but not on z and δ is the detuning, which is equivalent to the detuning f of Dirac solitons in the form of Eq. (3). This is the case in which the discrete solitons propagate parallel to the longitudinal axis z of BWAs and the normalized wave number can get three central values $Q = 0$ or $\pm\pi$ in the first Brillouin zone. By inserting the *Anstaz* (8) into Eq. (1), one can easily get the following system of algebraic equations:[13]

$$-\delta b_n + \kappa[b_{n+1} + b_{n-1}] - (-1)^n \sigma b_n + \gamma |b_n|^2 b_n = 0. \tag{9}$$

From Eq. (9), we can easily get the following subset of equations for even component b_{2n},

$$-\delta b_{2n} + \kappa[b_{2n+1} + b_{2n-1}] - \sigma b_{2n} + \gamma |b_{2n}|^2 b_{2n} = 0, \tag{10}$$

and subset of equations for odd component b_{2n+1},

$$-\delta b_{2n+1} + \kappa[b_{2n+2} + b_{2n}] + \sigma b_{2n+1} + \gamma |b_{2n+1}|^2 b_{2n+1} = 0, \tag{11}$$

which now has another sign in front of σ.

Before proceeding further, it is useful to mention two general transformation rules of discrete solitons:

First, when σ just changes its sign while all other parameters are fixed, we actually have the same physical system of BWAs, but now, all waveguide positions n are just shifted by one as mentioned in Sec. II. Therefore, the only difference in the system and the soliton solution is that the component, which was even before, now turns to odd and vice versa.

Second, suppose that b_{2n}, b_{2n-1}, and δ are the even component, the odd component, and the detuning of the discrete soliton, respectively; now, if we change the sign for both σ and γ, i.e., if $\sigma \to -\sigma$ and $\gamma \to -\gamma$, then from Eqs. (10) and (11), one can easily see that the discrete soliton will be now $b_{2n} \to b_{2n}$, $b_{2n-1} \to -b_{2n-1}$, and $\delta \to -\delta$; i.e., the odd component and the detuning will change their sign, while the even component is the same.

In the quasilinear regime, the intensity of all components is low; therefore, we can ignore the nonlinear term in Eqs. (1) and (9). In this quasilinear regime, it turns out that we can approximately find the beyond-band discrete solitons in a simple form of two hyperbolic functions for even and odd components as follows:

$$\begin{bmatrix} b_{2n} \\ b_{2n-1} \end{bmatrix} = \begin{bmatrix} p.\mathrm{sech}\left(\frac{2n}{n_0}\right) \\ q.\mathrm{sech}\left(\frac{2n-1}{n_0}\right) \end{bmatrix}, \tag{12}$$

where p and q are the peak amplitude of the even and odd components, respectively.

If we insert Eq. (12) into Eq. (10), then in the linear regime, we obtain the following relationship:

$$p(\delta_l + \sigma) = 2\kappa q, \tag{13}$$

where δ_l denotes the linear detuning δ in the absence of nonlinearity. Similarly, if we insert Eq. (12) into Eq. (11), then in the linear regime, we obtain the following relationship:

$$q(\delta_l - \sigma) = 2\kappa p. \tag{14}$$

If the central amplitude $b_0 = p$ is given at the waveguide with $n = 0$, then one can easily calculate two quantities δ_l and q from Eq. (13) and Eq. (14) as follows:

$$\delta_l = \pm\sqrt{\sigma^2 + 4\kappa^2}, \tag{15}$$

$$q = \frac{b_0\left(\sigma \pm \sqrt{\sigma^2 + 4\kappa^2}\right)}{2\kappa}. \tag{16}$$

The two limits of the linear spectrum calculated by Eq. (15) are marked by three points M_0, M_1, and M_{-1} in Fig. 1(b). As shown later in Fig. 5(b), if the nonlinearity is taken into account, then if γ is positive (negative), one has to get the positive (negative) sign in front of the square in Eqs. (15) and (16). As a result, if $\gamma > 0$, then from Eqs. (13) and (15), we can easily see that two peak amplitudes of the even and odd components (p and q) must have the same sign because $\delta_l + \sigma > 0$ and κ is always positive. This means that all the components (both even and odd) of these discrete solitons have just the *same* sign. Therefore, when $\gamma > 0$, the normalized wave number $Q = 0$, and the detuning δ of the nonlinear beyond-band discrete solitons increases if the central amplitude b_0 also increases [see two upper curves in Fig. 5(b)] as illustrated by the upward arrow starting from point M_0 in Fig. 1(b). On the contrary, if $\gamma < 0$, then p and q must have opposite signs because $\delta_l + \sigma < 0$; therefore, the even and odd components have *opposite* signs. Therefore, when $\gamma < 0$, the normalized wave number $Q = \pm\pi$, and the detuning δ of the nonlinear beyond-band discrete solitons decreases if the central amplitude b_0 increases [see two lower curves in Fig. 5(b)] as illustrated by two downward arrows starting from points M_{-1} and M_1 in Fig. 1(b). Note that the values of linear detuning δ_l in the form

of Eq. (15) are obviously located outside of the gap from $-|\sigma|$ to $|\sigma|$ created by the dispersion relationship (7). These linear detunings correspond to the case when the normalized wave number in Eq. (7) gets the values $Q = k\pi$ when k is a whole number, such as 0, ±1, ±2, ... Within the first Brillouin zone, our beyond-band discrete solitons in this work show that $Q = 0$ or $\pm\pi$ not only in the quasilinear regime [see Fig. 2(d)], but also in all ranges of the peak amplitudes. This is also different from Dirac solitons found in Ref. 13 where the normalized wave number is centered at $Q = \pm\pi/2$ [see Fig. 2(b) therein], which corresponds to the so-called Bragg angle of a beam launched into BWAs.[9,37] Note also that the discrete gap soliton in BWAs has been observed by launching two beams under two opposite Bragg angles with opposite inclinations.[25]

In general, it is difficult to derive the analytical soliton solutions for the system of nonlinear coupled-mode equations (1). In this case, one can use some numerical methods to find soliton solutions. In this work, we use the so-called shooting method[38] to search for a new class of discrete solitons by "shooting" from the BWA center at the site $n = 0$ to the two edges.

Thanks to the system symmetry as schematically illustrated in Fig. 1(a), we can look for discrete soliton solutions to Eq. (9) with the following property: $b_n = b_{-n}$. Therefore, if the center amplitude of the discrete soliton b_0 is given, then all other values of b_n can be calculated from Eq. (9). However, we just want to find *bright* discrete solitons with a bell-like shape where two wings decrease to zero when $n \to \pm\infty$. To achieve this aim, we just have to refine the detuning δ such that the condition $b_n \to 0$ is satisfied when $|n|$ is large enough. Therefore, the eigenvalue of the detuning δ of the discrete soliton will be a function of its center amplitude b_0. With this simple shooting method, we can numerically find all exact discrete solitons of the new class below in this work.

As an example, in Fig. 2(a), we plot the profile of a beyond-band discrete soliton in the quasilinear regime with $\sigma = -1$, $\gamma = 1$, and $\kappa = 1$ when we fix the central amplitude $b_0 = p = 0.1$. The upper blue curve with round markers and the lower black curve with round markers represent the even component b_{2n} and the odd component b_{2n-1} of the discrete soliton *numerically* calculated using the shooting method for Eq. (9), which gives us the detuning $\delta = 2.2402$.

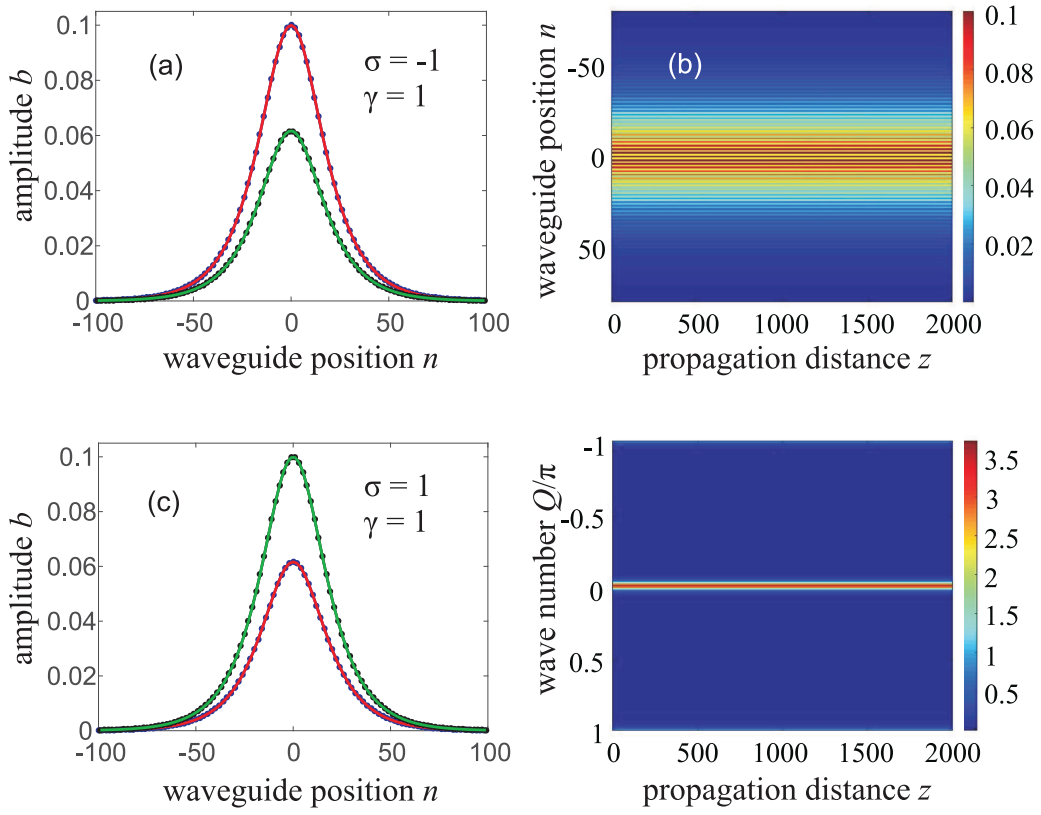

FIG. 2. A weak beyond-band discrete soliton with peak amplitude $b_0 = 0.1$. (a) The profile of this discrete soliton when $\sigma = -1$, $\gamma = 1$, $\delta = 2.2402$, and $\kappa = 1$. The two upper curves represent the even component b_{2n}, whereas the two lower curves represent the odd component b_{2n-1}. The curves with round markers are numerically calculated for the discrete soliton, which coincide well with the solid curves representing two *secant* functions. (b) Propagation of the discrete soliton whose input profile is plotted in (a). (c) The profile of another discrete soliton when all parameters are the same as in (a) with exceptions that $\sigma = 1$ and the central amplitude $b_0 \simeq 0.0617$ now. (d) Evolution of the spectra of the discrete soliton whose input profile is plotted in (c).

This value is quite close and just above point M_0 in Fig. 1(b) representing the theoretical value for the linear detuning $\delta_l = \sqrt{\sigma^2 + 4\kappa^2} = 2.2361$ shown in Eq. (15). As seen in Fig. 2(a), b_n has the same sign for all values of n; therefore, the normalized wave number of this beyond-band discrete soliton $Q = 0$. The upper red curve and the lower green curve in Fig. 2(a) are two fitted curves based on two hyperbolic *secant* functions with the width parameter $n_0 = 14.66$ and two peak amplitudes $p = b_0 = 0.1$ and $q = 0.0618$ as predicted by Eq. (16). As clearly seen in Fig. 2(a), the two fitted curves coincide perfectly well with two curves numerically calculated such that two latter curves would be totally hidden by the two former ones if we did not use the round markers for them. It is also clear from Fig. 2(a) that the even component of the new discrete soliton does not change its sign across the transverse direction of the BWA when n runs. This feature is also held true for the odd component of this new discrete soliton. This makes new discrete solitons totally different from Dirac solitons illustrated in Fig. 1 whose even (and odd) component constantly changes its sign when n runs.

In Fig. 2(b), we show the propagation of this discrete soliton using the initial condition, which is shown by two numerical curves with round markers in Fig. 2(a) for numerically integrating Eq. (1) along z. As seen in Fig. 2(b), which plots $|a_n(z)|$, this discrete soliton is stable and can conserve its profile perfectly well during propagation for a very long distance.

Now, we want to check the validity of the first transformation rule given in Sec. III in the quasilinear regime. In order to do that we look for a discrete soliton of the new class when $\sigma = 1$ and $\gamma = 1$, i.e., we just change the sign of σ while keeping all other parameters unchanged as compared to the case analyzed in Fig. 2(a). In order to obtain the profile of this discrete soliton using the shooting method and to verify the first transformation rule, we now fix the detuning of this soliton as the one analyzed in Fig. 2(a), i.e., $\delta = 2.2402$, then we refine the central amplitude b_0 until the moment when we obtain the localized structure, i.e., when $b_n \to 0$ if n is large enough. With this technique, the central amplitude is tuned to be $b_0 \simeq 0.0617$ [which turns out to be practically the same value for $q = 0.0618$ of the fitted lower curve for the discrete soliton shown in Fig. 2(a)]. The profile of this beyond-band discrete soliton is shown in Fig. 2(c) where the upper black curve with round markers now plots the *odd* component b_{2n-1} and the lower blue curve with round markers plots the *even* component b_{2n} of the new discrete soliton calculated by the shooting method. In Fig. 2(c), we also plot two fitted curves using Eq. (12) where $p = b_0 \simeq 0.0617$, $q = 0.1$, which is practically the same as the value $q = 0.0998$ calculated by Eq. (16), and n_0 is also equal to 14.66 as two fitted curves in Fig. 2(a). In short, everything is the same as in Fig. 2(a) with the only exception that the peaks p and q swap their values because the even component of one soliton is the odd component of the other soliton and vice versa, as expected from the first transformation rule.

In Fig. 2(d), we show the propagation of the spectra of the discrete soliton whose profile is plotted in Fig. 2(c). This profile is first used as the initial condition for numerically integrating Eq. (1) along z to obtain $a_n(z)$. We then use the Fourier transformation $a_n(z) \to \tilde{a}(Q, z)$ to calculate the spectra of the discrete soliton by going from the spatial domain n into the normalized wave number domain Q at each z. As seen in Fig. 2(d), the spectra of this discrete soliton are just centered around the normalized wave number $Q = 0$ as discussed below Eq. (16) for beyond-band discrete solitons in the quasilinear regime. This is understandable because all components (both even and odd) of these solitons have the same sign when n runs; therefore, we should have $Q = 0$ as shown by Eq. (6). Note that these spectra are also stable and can conserve their profile perfectly well during propagation for a very long distance as seen in Fig. 2(d).

We want to stress that we always set the nonlinear coefficient $\gamma = 1$ (not 0) for calculating the profiles of two discrete solitons in Figs. 2(a) and 2(c) and simulating their propagation in Figs. 2(b) and 2(d). Therefore, Fig. 2 represents a good example of new beyond-band discrete solitons in the quasilinear regime when the nonlinear coefficient $\gamma \neq 0$, but the peak amplitude is low so that they operate as in the linear regime.

IV. BEYOND-BAND DISCRETE SOLITONS WITH ENHANCED NONLINEARITY

In this section, we look for beyond-band discrete solitons when the nonlinearity of Kerr type is enhanced, i.e., when their peak amplitudes are not low anymore. In Fig. 3(a), we show the profile of a discrete soliton with the central amplitude $b_0 = 0.4$ with the following set of parameters: $\sigma = -1$, $\gamma = 1$, and $\kappa = 1$. Like in Fig. 2(a), the upper blue curve with round markers representing the even component and the lower black curve with round markers representing the odd component are both numerically calculated by the shooting method, whereas the red curve and the green one are two fitted curves in the form of two hyperbolic secant functions as shown by Eq. (12) with now $p = b_0 = 0.4$, $n_0 = 3.6$, and $q = 0.2362$, which is different, as expected, from the value $q = 0.2472$ provided by Eq. (16) in the linear regime. The detuning of this discrete soliton is calculated to be $\delta = 2.3004$, which is also significantly different from the linear detuning $\delta_l = 2.2361$ obtained from Eq. (15). Therefore, the detuning of this soliton with $\gamma > 0$ is represented by a point in the upward arrow in Fig. 1(b), which is noticeably higher than point M_0 therein. Note that the normalized wave number Q of this soliton is also equal to zero as shown in Fig. 3(e) and discussed below. We can see from Fig. 3(a) that two hyperbolic secant functions can appropriately fit their corresponding numerical curves, but not perfectly well. This is different from the situation shown in Figs. 2(a) and 2(c) where the fitted curves perfectly well coincide with their numerical curves. This difference can be easily noticed if we enlarge both Figs. 2(a), 2(c), and 3(a) in the electronic version of this paper. For instance, in Fig. 3(a), the upper red fitted curve is wider at the top but narrower at the bottom as compared to the upper blue curve with round markers. Meanwhile, the lower green fitted curve is always narrower than its numerical black curve with round markers, both at the top and at the bottom. This kind of deviation between the fitted curves and exactly calculated curves will become more pronounced if the peak amplitude of the discrete solitons gets higher.

In Fig. 3(a), we plot the profile of the new discrete soliton when $\sigma = -1$ and $\gamma = 1$. Now, we change both signs of these two parameters at the same time and plot the profile of the new discrete soliton in Fig. 3(c) with central amplitude $b_0 = 0.4$ as in Fig. 3(a). As exactly dictated by the second transformation rule given in Sec. III, the detuning of this new discrete soliton is $\delta = -2.3004$, which has the

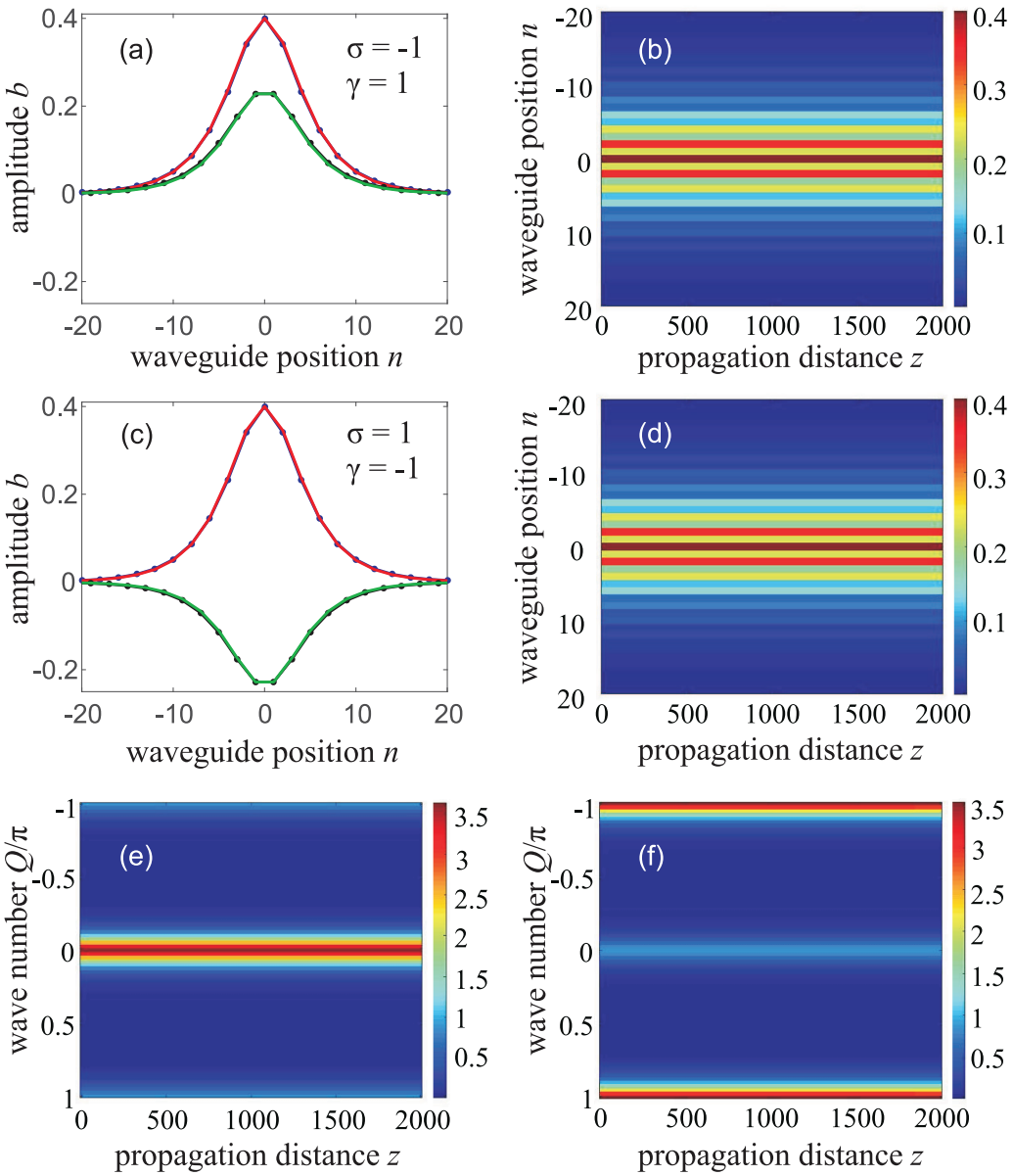

FIG. 3. (a) The profile of a beyond-gap discrete soliton with peak amplitude $b_0 = 0.4$ when $\sigma = -1$, $\gamma = 1$, $\delta = 2.3004$, and $\kappa = 1$. The two upper curves represent the even component b_{2n}, whereas the two lower curves represent the odd component b_{2n-1}. The curves with round markers are numerically calculated for the discrete soliton, which coincide well with the solid curves representing two secant functions. (b) Propagation of the discrete soliton whose input profile is plotted in (a). (c) The same as (a) but now, we switch the signs such that $\sigma = 1$, $\gamma = -1$; therefore, $\delta = -2.3004$. (d) Propagation of the discrete soliton whose input profile is plotted in (c). (e) Evolution of the spectra of the discrete soliton analyzed in (a) and (b). (f) Evolution of the spectra of the discrete soliton analyzed in (c) and (d).

same absolute value but with the opposite sign of the detuning of the discrete soliton plotted in Fig. 3(a). Therefore, the detuning of this soliton with $\gamma < 0$ is represented by two points in two downward arrows in Fig. 1(b), which are noticeably lower than two points M_{-1} and M_1 therein. Note that the normalized wave number Q of this soliton is centered around $\pm\pi$ as shown in Fig. 3(f) and discussed below. Moreover, from Figs. 3(a) and 3(c), we can clearly see that the even components b_{2n} of these two discrete solitons are absolutely the same, whereas their odd components b_{2n-1} are just different in their signs, as exactly dictated by the second transformation rule.

In Figs. 3(b) and 3(d), we show the propagation of two discrete solitons using numerical curves plotted in Figs. 3(a) and 3(c),

respectively, as the initial conditions for numerically integrating Eq. (1) along z. As seen in Figs. 3(b) and 3(d), which plot $|a_n(z)|$, these two discrete solitons are also stable and can conserve their profile perfectly well during propagation for a very long distance.

In Fig. 3(e), we show the propagation of the spectra of the discrete soliton analyzed in Figs. 3(a) and 3(b). As seen in Fig. 3(e), the spectra of this discrete soliton are mainly centered around the normalized wave number $Q = 0$ just like the solitons in Fig. 2 because all components of these solitons have the same sign. Note that the spectra of the soliton shown in Fig. 2 are much narrower than those in Fig. 3(e) because of the difference in the spatial width of these solitons.

In Fig. 3(f), we show the propagation of the spectra of the discrete soliton analyzed in Figs. 3(c) and 3(d). As seen in Fig. 3(f), the spectra of this discrete soliton are now mainly centered around the normalized wave number $Q = \pm\pi$ because, as shown in Fig. 3(c), b_n constantly changes its sign when n runs, which is equivalent to the situation when $Q = \pm\pi$ as shown by Eq. (6).

Now, we want to look for a discrete soliton of the new class when $\sigma = 1$ and $\gamma = 1$; i.e., we just change the sign of σ while keeping all other parameters unchanged as compared to the case analyzed in Fig. 3(a). As expected, this situation must completely obey the first transformation rule given in Sec. III. In order to obtain the profile of this discrete soliton using the shooting method and to verify the first transformation rule, we now fix the detuning of this soliton as the one analyzed in Fig. 3(a); i.e., $\delta = 2.3004$, then, we refine the central amplitude b_0 until the moment when we obtain the localized structure, i.e., when $b_n \to 0$ if n is large enough. With this technique, the central amplitude is tuned to be $b_0 \simeq 0.2363$ [which turns out to be the same value for q of the fitted lower curve for the discrete soliton shown in Fig. 3(a)], and the profile b_n of this new discrete soliton is shown in Fig. 4(a).

In Fig. 4(b), the upper black curve with round markers plots the odd component b_{2n-1}, whereas the lower blue curve with round markers plots the even component b_{2n} of the new discrete soliton calculated by the shooting method. In Fig. 4(b), we also plot two fitted curves using Eq. (12) where $p \simeq 0.2363$ is now equal to the central amplitude b_0, $q = 0.4$, and $n_0 = 3.6$. In short, everything is the same as in Fig. 3(a) with the only exception that the peaks p and q swap their values. Note that, like in Fig. 3(a), these two analytical curves can only appropriately fit the two numerical curves in Fig. 4(b), but not perfectly well. To better show the validity of the first transformation rule, in Fig. 4(c), we plot four curves: the purple one is the profile of the new discrete soliton taken from Fig. 4(a) when $\sigma = 1$ and $\gamma = 1$, the upper black curve and the lower blue curve are the odd b_{2n-1} and even components b_{2n} of this discrete soliton (which are the upper and lower envelopes of b_n), and the dashed green curve is the profile b_n of the discrete soliton analyzed in Fig. 3(a) when $\sigma = -1$ and $\gamma = 1$. As clearly seen in Fig. 4(c), the two envelopes of the discrete soliton with $\sigma = 1$ and $\gamma = 1$ are also the envelopes of the discrete soliton with $\sigma = -1$ and $\gamma = 1$ with the *only* difference that the even component of one soliton is the odd component of the other soliton and vice versa, as expected from the first transformation rule.

In Fig. 4(d), we show the propagation of the discrete soliton using b_n plotted in Fig. 4(a) as the initial condition for numerically integrating Eq. (1) along z. As seen in Fig. 4(d), which shows $|a_n(z)|$, this discrete soliton is also stable and can conserve their profile perfectly well during propagation for a very long distance.

In Fig. 5(a), we show the even (upper curve) and odd (lower curve) components of a beyond-band discrete soliton when $\sigma = -1$ and $\gamma = -1$, i.e., when both of these parameters change the sign as compared to the case shown in Fig. 4(a). As predicted by the second transformation rule, one can find a new discrete soliton in this case just by changing the sign of both the detuning and the odd component b_{2n-1} while keeping the even component and other parameters the same as in the case of the discrete soliton analyzed in Fig. 4. Indeed, the second transformation rule is once again verified in this case as one can clearly see the profile of this new discrete soliton in Fig. 5(a) with its detuning is $\delta = -2.3004$ and all properties dictated by the second transformation rule. This discrete soliton is also stable, which can propagate for a very long distance without any distortion of its profile.

Note also that profiles of the discrete soliton shown in Fig. 5(a) and the one shown in Fig. 3(c) also obey the first transformation rule when σ changes its sign, while γ and other parameters are unchanged. Therefore, these discrete solitons of the new type must have the same detuning $\delta = -2.3004$, while their even and odd components just swap each other.

Therefore, now, it is clear to us that each of the even and odd components of all beyond-band discrete solitons found in this work does not change its sign when n runs. This is one of their distinguishing features. Because of this property, each of functions Ψ_1 and Ψ_2 of the two-component spinor appearing in the Dirac equation (5) constantly changes its sign when n runs (or when its corresponding variable ξ jumps with a step equal to unity). Therefore, the derivative $\partial_\xi \Psi$ in the Dirac equation (5) does not make any mathematical sense in this case. Therefore, *unlike* the Dirac solitons, all beyond-band discrete solitons found in this work are just solutions to the coupled-mode equation (1) describing light evolution in BWAs but cannot be approximate solutions to the Dirac equation (5). Because, as mentioned above, each of the even and odd components of all beyond-band discrete solitons found in this work does not change its sign when n runs, and each of these two components can be regarded as an unstaggered soliton. Therefore, we can say that these beyond-band discrete solutions are out-gap unstaggered–unstaggered solitons in two-component BWAs. Note that unstaggered–staggered solitons have been found in two-component discrete nonlinear Schrödinger lattices where the unstaggered component is coupled to the staggered one whose sign constantly changes when n runs.[33,34] In this context, Dirac solitons described by Eq. (3) can be considered staggered–staggered solitons.

In the rest of this work, we want to further study the detuning δ of beyond-band discrete solitons. In Fig. 5(b), we plot the dependence of the detuning δ as a function of the central amplitude b_0 for all four combinations of signs of σ and γ. Two dotted horizontal cyan curves show the linear limits of the detuning $\delta_l = \pm\sqrt{\sigma^2 + 4\kappa^2} = \pm 2.2361$ as provided by Eq. (15) and marked by three points M_0, M_1, and M_{-1} in Fig. 1(b). The space between the upper dotted horizontal cyan curve and the top of the bandgap in Fig. 5(b) is the upper band ω_+ of linear plane waves in BWAs, which correspond to the upper green band in Fig. 5(b). Meanwhile, the space between the lower dotted horizontal cyan curve and the

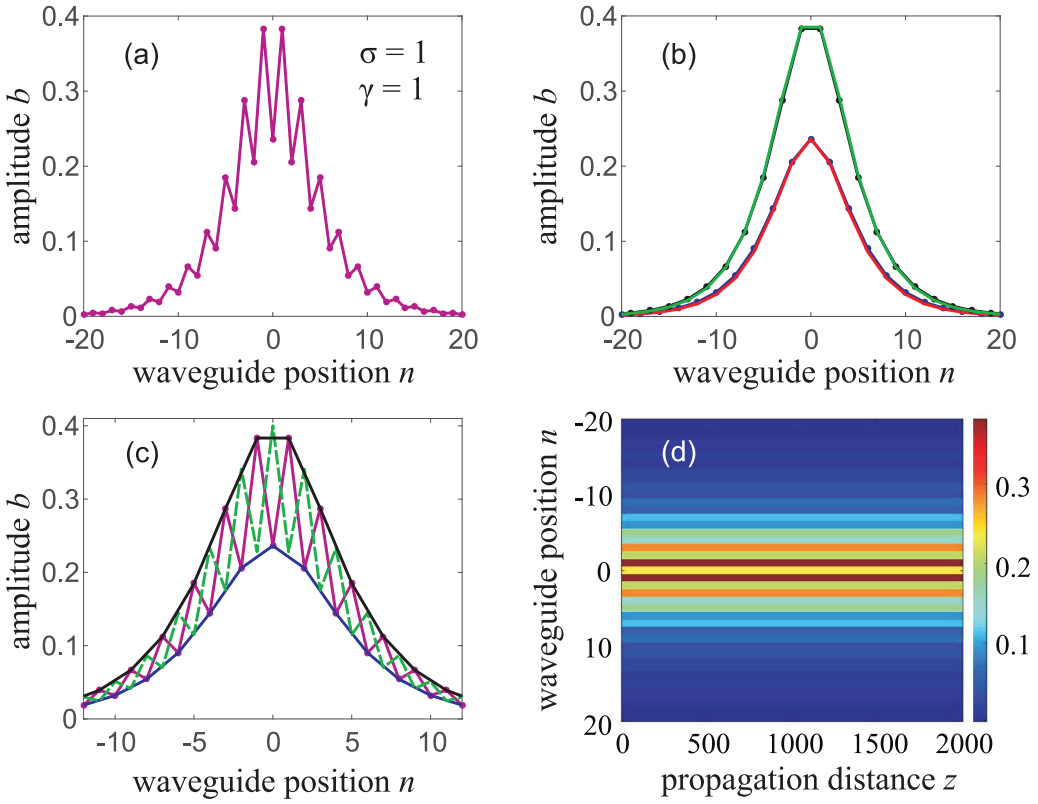

FIG. 4. (a) The profile of a beyond-band discrete soliton with peak amplitude $b_0 = 0.2363$ when $\sigma = 1$, $\gamma = 1$, $\delta = 2.3004$, and $\kappa = 1$. (b) The two upper curves represent the odd component b_{2n-1}, whereas the two lower curves represent the even component b_{2n} of this discrete soliton. The curves with round markers are numerically calculated for the discrete soliton, which coincide well with the solid curves representing two secant functions. (c) The profile and two components (even and odd) of this discrete soliton are plotted together with the profile of the discrete soliton (dashed line) analyzed in Fig. 3. (d) Propagation of the discrete soliton whose input profile is plotted in (a).

bottom of the bandgap in Fig. 5(b) is the lower band ω_- of linear plane waves in BWAs, which correspond to the lower green band in Fig. 5(b). Apart from these two analytical curves showing δ_l, all other four curves in Fig. 5(b) are calculated by the shooting method and then verified by the two transformation rules given in Sec. III. Indeed, the top solid blue curve with $\sigma = 1$ and $\gamma = 1$ is totally symmetrical to the bottom blue curve with round markers when $\sigma = -1$ and $\gamma = -1$ with respect to the zero-level axis. In order to verify this symmetry, we also plot the mirror image (bottom solid red curve) of the top solid blue curve through the zero-level axis in Fig. 5(b), and we can clearly see that the bottom blue curve with round markers absolutely coincides with this mirror image. This symmetry is also true for two curves: the solid green one (when $\sigma = -1$ and $\gamma = 1$) and the green curve with round markers (when $\sigma = 1$ and $\gamma = -1$) where the latter completely coincides with the mirror image (solid black curve) of the former.

As expected, when the central amplitude b_0 decreases toward zero, all the four numerical curves asymptomatically reach the two linear limits of the detuning (two horizontal dotted curves) given by Eq. (15). As clearly seen in Fig. 5(b), all these new discrete solitons are out-gap because their detunings δ lie outside of the bandgap from $-|\sigma|$ to $|\sigma|$, which is represented by the gray region. They are also located just above the upper band ω_+ of linear plane waves in BWAs if γ is positive or below the lower band ω_- of linear plane waves in BWAs if γ is negative. That is the reason why we propose to use the term *beyond-band* for them. Note that the detuning δ of the new discrete solitons is always positive if the nonlinear coefficient γ is positive. On the contrary, if $\gamma < 0$, then δ of all new discrete solitons is negative. Note also that two discrete solitons with the same detuning δ but opposite σ shown in Fig. 5(b) can be considered one discrete soliton obeying the first transformation rule when its even and odd components swap each other [as the case shown in Figs. 3(a) and 4 or the case shown in Figs. 3(c) and 5(a)]. As discussed above, the normalized wave numbers Q of these beyond-band discrete solitons are just centered around 0 (when the nonlinear coefficient $\gamma > 0$) or $\pm\pi$ (when $\gamma < 0$). Therefore, all three upper curves in Fig. 5(b) are represented by the upward arrow shown in Fig. 1(b), whereas all three lower curves in Fig. 5(b) are represented by two downward arrows shown in Fig. 1(b).

In Fig. 5(c), we plot the dependence of the Hamiltonian H as a function of the detuning δ for two beyond-band discrete solitons with $\gamma = 1, \kappa = 1, \sigma = 1$ (upper curve) and $\sigma = -1$ (lower curve).

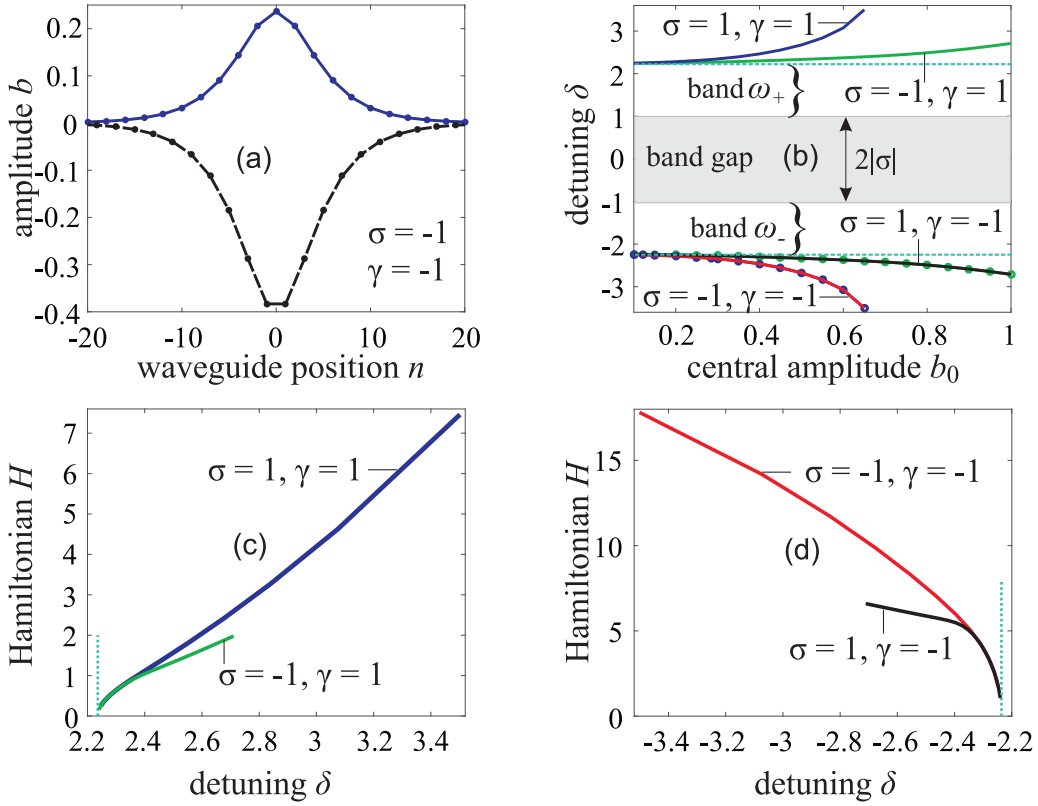

FIG. 5. (a) The even component b_{2n} (upper curve) and the odd component b_{2n-1} (lower curve) of a beyond-band discrete soliton with central amplitude $b_0 \simeq 0.2363$ when $\sigma = -1$, $\gamma = -1$, $\delta = -2.3004$, and $\kappa = 1$. (b) The dependence of the detuning δ as a function of the central amplitude b_0 for different sets of parameters σ and γ, while κ is also equal to unity. Two dotted horizontal lines in (b) plot two limits of the linear detuning $\delta_l = \pm\sqrt{\sigma^2 + 4\kappa^2}$. The gray region in (b) is the bandgap spanning from $-|\sigma|$ to $|\sigma|$ of linear plane waves in BWAs. (c) and (d) The dependence of the Hamiltonian H as a function of the detuning δ when $\gamma = 1$ and -1, respectively. Two dotted vertical lines in (c) and (d) denote two values of the linear detuning δ_l. Parameters for (b)–(d): $\gamma = \pm 1$, $\kappa = 1$, and $\sigma = \pm 1$.

The dotted vertical cyan curve in Fig. 5(c) denotes the position of the linear detuning $\delta_l = 2.2361$. These three curves in Fig. 5(c) correspond to three upper curves with positive δ in Fig. 5(b). Analogously, in Fig. 5(d), we plot the dependence of H as a function of δ for two beyond-band discrete solitons with $\gamma = -1$. The dotted vertical cyan curve in Fig. 5(d) denotes the position of the linear detuning $\delta_l = -2.2361$. These three curves in Fig. 5(d) correspond to three lower curves with negative δ in Fig. 5(b). We want to emphasize that when the peak amplitude of beyond-band discrete solitons decreases to zero, their detunings will asymptotically reach the linear detuning $\delta_l = \pm\sqrt{\sigma^2 + 4\kappa^2}$ as clearly shown in Figs. 5(b)–5(d). This feature makes the beyond-band discrete solitons analyzed in this work different from the discrete on-top breathers analyzed in Ref. 29 because these breathers cannot be continued in frequency down (up) to the linear spectrum for positive (negative) γ.

So far, we have analyzed the beyond-band discrete solitons in the parameter range when $|\gamma| = 1$, $|\sigma| = 1$, and $\kappa = 1$; i.e., their absolute values are all equal to each other. Now, we want to investigate the situation in a different parameter range when both σ and κ are much smaller than $|\gamma|$, which can happen if the nonlinear-index coefficient n_2 of waveguides is large. In this situation, even a very weak amplitude of signals can undergo enhanced nonlinear effects. To be specific, we now use $|\sigma| = 0.1$, $\kappa = 0.02$, but $\gamma = 1$. These parameters are exactly the same as those in Ref. 29 where the discrete on-top breathers were analyzed (see Fig. 8 therein). In Fig. 6(a), we plot two curves showing the dependence of the detuning δ as a function of the central amplitude b_0 for two values of σ with opposite signs. The dotted horizontal cyan curve in Fig. 6(a) shows the linear limit of the detuning $\delta_l = \sqrt{\sigma^2 + 4\kappa^2} = 0.1077$, which completely corresponds to the limit $\omega_u = 1.1477$ calculated by Eq. (9) in Ref. 29 (the difference between these two linear limits is $1 + 2\kappa$ due to the structure difference of governing equations in these two works). In Fig. 6(b), we plot the dependence of the Hamiltonian H as a function of the detuning δ for two values $\sigma = \pm 0.1$. The dotted vertical cyan curve in Fig. 6(b) denotes the position of the linear limit $\delta_l = 0.1077$. As clearly shown in Fig. 6, the detuning of discrete solitons can get as close as desired to the linear limit δ_l if we decrease the central amplitude b_0 to zero. Note that the discrete on-top breathers analyzed in Ref. 29 do not have this feature [see four lower curves in Fig. 8(a) therein].

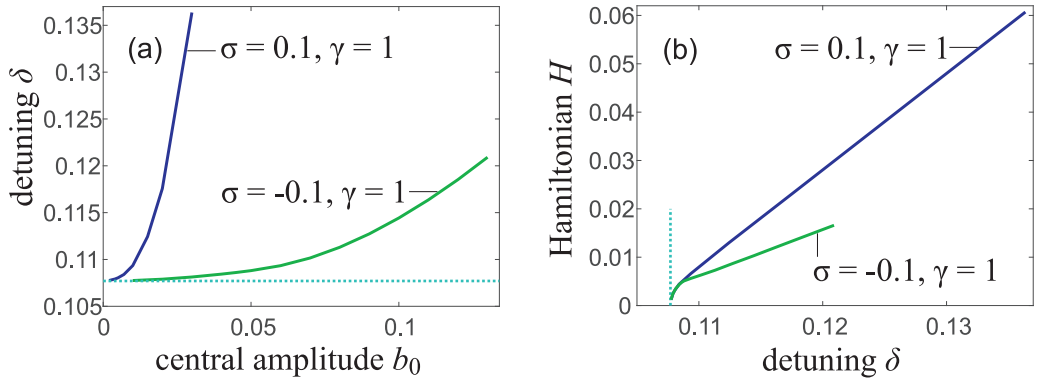

FIG. 6. (a) The dependence of the detuning δ as a function of the central amplitude b_0. The dotted horizontal line in (a) shows the limit of the linear detuning $\delta_l = \sqrt{\sigma^2 + 4\kappa^2} = 0.1077$. (b) The dependence of the Hamiltonian H as a function of the detuning δ. The dotted vertical line in (b) denotes $\delta_l = 0.1077$. Parameters: $\gamma = 1$, $\kappa = 0.02$, and $\sigma = \pm 0.1$.

As mentioned above, because γ in Fig. 6 is much larger than both σ and κ, therefore, even when the central amplitude b_0 is small (for instance, $b_0 = 0.1$), these discrete solitons are under action of strong nonlinearity. This can be seen in Fig. 6(a) when their detunings are quite far from the linear limit δ_l and far from each other instead of being close to δ_l and close to each other as shown in Fig. 5(b). The beam profiles of these solitons (not shown here) are localized just in a few waveguides instead of spreading out widely as shown in Fig. 2(b). Note that in Fig. 6, we just focus in the case with $\gamma = 1$. If we switch the sign of γ, we will also obtain pictures, which are qualitatively similar to Figs. 5(b)–5(d).

It is worth mentioning that the beyond-band discrete solitons investigated in this work are also different from the discrete embedded solitons reported in Ref. 35 and embedded solitons in a continuous model reported in Ref. 39. These localized embedded solitons (both discrete and continuous) are isolated solitary waves, existing at *discrete* values of the propagation constant inside the continuous spectrum of linear waves.[35,39] On the contrary, as clearly shown in Figs. 1(b), 5(b), and 6, the beyond-band discrete solitons investigated in this work have *continuous* values of the detuning δ, which is the correction to their propagation constant ω [see Eqs. (6) and (8)]. Moreover, unlike embedded solitons, the continuous values δ of these beyond-band discrete solitons are not located inside the continuous spectrum $\omega_\pm$ of linear waves, but beyond-band in the sense that the detuning δ is above the band ω_+ if γ is positive and δ is below the band ω_- if γ is negative as clearly shown in Figs. 1(b) and 5(b).

V. CONCLUSIONS

In conclusion, we have demonstrated the existence of a completely new class of *beyond-band* discrete solitons in BWAs with Kerr nonlinearity whose detunings are located out of the bandgap (out-gap) and beyond the two bands of the linear plane waves. The even and odd components of these discrete solitons can be appropriately approximated by two hyperbolic *secant* functions. This approximation is perfectly good in the quasilinear regime when their peak intensity is low. In this case, the detuning and two peaks of these two *secant* functions can be simply obtained by analytical formulas. If the peak intensity becomes higher, then this approximation is still satisfactory, but not perfectly good anymore. These new beyond-band discrete solitons are different from all other discrete solitons investigated earlier in BWAs because they simultaneously possess three features: (i) their normalized wave numbers Q are just centered around 0 (when the nonlinear coefficient $\gamma > 0$) or $\pm\pi$ (when $\gamma < 0$); (ii) each of their even and odd components, as a result of (i), does not change their signs across the transverse direction of BWAs when n runs (specifically, all components have the same sign if $\gamma > 0$, whereas the even and odd components have opposite signs if $\gamma < 0$); and (iii) their frequency can asymptotically reach the linear spectrum when their peak amplitude decreases to zero. We have also provided two general transformation rules, which can help us from a beyond-band discrete soliton to construct all the other ones for different combinations of signs of the propagation mismatch σ and nonlinear coefficient γ.

ACKNOWLEDGMENTS

This work was funded by Vingroup and supported by Vingroup Innovation Foundation (VINIF) under Project Code VINIF.2021.DA00001. M. C. Tran is thankful to the Van Lang University.

AUTHOR DECLARATIONS

Conflict of Interest

The authors have no conflicts to disclose.

Author Contributions

Minh C. Tran: Investigation (supporting); Software (equal). **Truong X. Tran:** Conceptualization (lead); Data curation (lead); Formal analysis (lead); Investigation (lead); Methodology (lead); Project administration (lead); Software (lead); Supervision (lead); Writing – review and editing (lead).

DATA AVAILABILITY

The data that support the findings of this study are available from the corresponding author upon reasonable request.

REFERENCES

[1]D. N. Christodoulides, F. Lederer, and Y. Silberberg, Nature **424**, 817–823 (2003).
[2]A. L. Jones, J. Opt. Soc. Am. **55**, 261–269 (1965).
[3]D. N. Christodoulides and R. I. Joseph, Opt. Lett. **13**, 794–796 (1988).
[4]Tr. X. Tran and F. Biancalana, Phys. Rev. Lett. **110**, 113903 (2013).
[5]D. N. Christodoulides and E. D. Eugenieva, Phys. Rev. Lett. **87**, 233901 (2001).
[6]U. Peschel, T. Pertsch, and F. Lederer, Opt. Lett. **23**, 1701–1703 (1998).
[7]T. Pertsch, P. Dannberg, W. Elflein, A. Bräuer, and F. Lederer, Phys. Rev. Lett. **83**, 4752 (1999).
[8]M. Ghulinyan, C. J. Oton, Z. Gaburro, L. Pavesi, C. Toninelli, and D. S. Wiersma, Phys. Rev. Lett. **94**, 127401 (2005).
[9]F. Dreisow, M. Heinrich, R. Keil, A. Tünnermann, S. Nolte, S. Longhi, and A. Szameit, Phys. Rev. Lett. **105**, 143902 (2010).
[10]S. Longhi, Phys. Rev. B **81**, 075102 (2010).
[11]F. Dreisow, R. Keil, A. Tünnermann, S. Nolte, S. Longhi, and A. Szameit, Europhys. Lett. **97**, 10008–10013 (2012).
[12]M. C. Tran, Q. Nguyen-The, C. C. Do, and Tr. X. Tran, Phys. Rev. A **105**, 023523 (2022).
[13]Tr. X. Tran, S. Longhi, and F. Biancalana, Ann. Phys. **340**, 179–187 (2014).
[14]Tr. X. Tran, X. N. Nguyen, and D. C. Duong, J. Opt. Soc. Am. B **31**, 1132–1136 (2014).
[15]Tr. X. Tran, X. N. Nguyen, and F. Biancalana, Phys. Rev. A **91**, 023814 (2015).
[16]Tr. X. Tran and D. C. Duong, Ann. Phys. **361**, 501–508 (2015).
[17]Tr. X. Tran and D. C. Duong, Chaos **28**, 013112 (2018).
[18]Tr. X. Tran, J. Opt. Soc. Am. B **36**, 2001–2006 (2019).
[19]Tr. X. Tran and F. B. Biancalana, Phys. Rev. A **96**, 013831 (2017).
[20]Tr. X. Tran, Chaos **30**, 063134 (2020).
[21]S. Longhi, Phys. Rev. A **81**, 022118 (2010).
[22]F. Dreisow, S. Longhi, S. Nolte, A. Tünnermann, and A. Szameit, Phys. Rev. Lett. **109**, 110401 (2012).
[23]Tr. X. Tran, H. M. Nguyen, and D. C. Duong, Phys. Rev. A **105**, 032201 (2022).
[24]A. A. Sukhorukov and Y. S. Kivshar, Opt. Lett. **27**, 2112–2114 (2002).
[25]A. A. Sukhorukov and Y. S. Kivshar, Opt. Lett. **28**, 2345–2347 (2003).
[26]M. Conforti, C. De Angelis, and T. R. Akylas, Phys. Rev. A **83**, 043822 (2011).
[27]R. Morandotti, D. Mandelik, Y. Silberberg, J. S. Aitchison, M. Sorel, D. N. Christodoulides, A. A. Sukhorukov, and Y. S. Kivshar, Opt. Lett. **29**, 2890–2892 (2004).
[28]M. Johansson, K. Kirr, A. S. Kovalev, and L. Kroon, Phys. Scr. **83**, 065005 (2011).
[29]A. Gorbach and M. Johansson, Eur. Phys. J. D **29**, 77–93 (2004).
[30]M. Johansson and A. Gorbach, Phys. Rev. E **70**, 057604 (2004).
[31]Y. S. Kivshar and N. Flytzanis, Phys. Rev. A **46**, 7972 (1992).
[32]Y. Nogami, F. M. Toyama, and Z. Zhao, J. Phys. A: Math. Gen. **28**, 1413–1424 (1995).
[33]B. A. Malomed, D. J. Kaup, and R. A. Van Gorder, Phys. Rev. E **85**, 026604 (2012).
[34]R. A. Van Gorder, A. L. Krause, B. A. Malomed, and D. J. Kaup, Commun. Nonlinear Sci. Numer. Simul. **85**, 105244–105258 (2020).
[35]K. Yagasaki, A. R. Champneys, and B. A. Malomed, Nonlinearity **18**, 2591–2613 (2005).
[36]S. Longhi, Opt. Lett. **35**, 235–237 (2010).
[37]F. Lederer, G. I. Stegeman, D. N. Christodoulides, G. Assanto, M. Segev, and Y. Silberberg, Phys. Rep. **463**, 1–126 (2008).
[38]N. N. Rosanov and Tr. X. Tran, Chaos **17**, 037114 (2007).
[39]J. Yang, B. A. Malomed, and D. J. Kaup, Phys. Rev. Lett. **83**, 1958 (1999).